

Proximity and Visuotactile Point Cloud Fusion for Contact Patches in Extreme Deformation

Jessica Yin^{1*}, Paarth Shah², Naveen Kuppaswamy², Andrew Beaulieu², Avinash Uttamchandani², Alejandro Castro², James Pikul^{1*}, and Russ Tedrake^{2*}

Abstract—Equipping robots with the sense of touch is critical to emulating the capabilities of humans in real world manipulation tasks. Visuotactile sensors are a popular tactile sensing strategy due to data output compatible with computer vision algorithms and accurate, high resolution estimates of local object geometry. However, these sensors struggle to accommodate high deformations of the sensing surface during object interactions, hindering more informative contact with cm-scale objects frequently encountered in the real world. The soft interfaces of visuotactile sensors are often made of hyperelastic elastomers, which are difficult to simulate quickly and accurately when extremely deformed for tactile information. Additionally, many visuotactile sensors that rely on strict internal light conditions or pattern tracking will fail if the surface is highly deformed. In this work, we propose an algorithm that fuses proximity and visuotactile point clouds for contact patch segmentation that is entirely independent from membrane mechanics. This algorithm exploits the synchronous, high spatial resolution proximity and visuotactile modalities enabled by an extremely deformable, *selectively transmissive* soft membrane, which uses visible light for visuotactile sensing and infrared light for proximity depth. We present the hardware design, membrane fabrication techniques, and evaluation of our contact patch algorithm in low (10%), medium (60%), and high (100%+) membrane strain states. We compare our algorithm against three baselines: proximity-only, tactile-only, and a first principles membrane mechanics model. Our proposed algorithm outperforms all baselines with an average root-mean-square error (RMSE) under 2.8 mm of the contact patch geometry across all strain ranges. We demonstrate our contact patch algorithm in four applications: varied stiffness membranes, torque and shear-induced wrinkling, closed loop control for whole body manipulation, and pose estimation.

I. INTRODUCTION

Humans are capable of an exceptionally diverse range of manipulation tasks, effortlessly able to pivot from the precise and delicate motion of threading a needle to the forceful whole-body coordination needed to carry another person. The critical role of human skin and sense of touch in the successful execution of these tasks has long been studied with the goal of reproducing human-like manipulation abilities in robots, motivating the rigorous development of electronic skins and tactile sensors [1]–[3]. Although there has been much progress,

¹Department of Mechanical Engineering and Applied Mechanics and GRASP Lab at University of Pennsylvania, Philadelphia, PA, USA.

²Toyota Research Institute, Cambridge, MA, USA.

*Corresponding authors: jessyin@seas.upenn.edu, pikul@seas.upenn.edu, russ.tedrake@tri.global

This work was supported in part by the National Science Foundation Graduate Research Fellowship Program under Grant No. 202095381 and by the National Science Foundation Emerging Frontiers in Research and Innovation (EFRI) award #1935294.

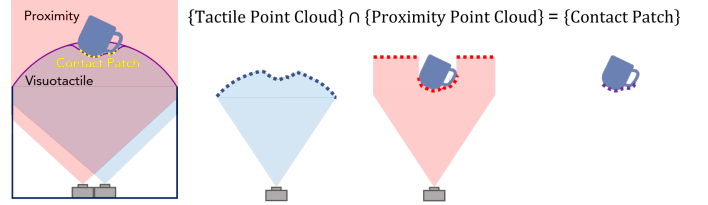


Fig. 1. Illustration of the key idea in fusing proximity and visuotactile point clouds for contact patch segmentation: the set of contact patch points is the intersection of the set of tactile points and the set of proximity points.

achieving the scalability, coverage, resolution, and compliance of human skin in tactile sensors for robots remains a challenge.

Recently, visuotactile sensors [4]–[9] have gained popularity as a tactile sensing strategy due to sensor coverage and resolution that scales with camera field-of-view and pixel count rather than number of sensing elements, as well as compatibility with powerful data processing techniques from computer vision. These sensors use a camera to observe a pattern on a deformable surface, which distorts upon contact. The images of the pattern distortion can inform contact information, such as shear, force, and object geometry.

However, despite leveraging a soft surface as the contact interface, visuotactile sensors rely on sensing mechanisms or data processing techniques that lose functionality beyond small deformations, typically less than 1 mm. For example, dot tracking and optical flow algorithms used to estimate depth or track motion [10]–[13] in these sensors are not robust to either occlusions or the large marker displacements that occur during high deformations of soft surfaces. Additionally, photometric stereo and frustrated-internal-reflection methods [14], [15] to estimate depth are heavily dependent on strict lighting conditions that fail when the soft material is highly deformed and too much light is released or the contact area is not evenly illuminated. Because these depth estimation methods limit the depth of object penetration, these sensors use a rigid backplate to prevent further deformation. This creates a critical challenge for visuotactile sensors by fundamentally restricting how much conformal contact can be made with the object.

The lack of conformal contact notably leads to very small contact patches that are not innately useful for pose estimation of cm-scale objects without additional nontrivial implementations of tactile exploration policies [16], [17], extensively training data-driven pose estimation frameworks with experimental or simulated data [18], [19], or integrating external

vision sensors in a perception pipeline [20], [21]. While small contact patches may be acceptable for small, mm-scale, distinctly featured objects like screws and nuts, general real-world manipulation demands greater versatility and frequent interactions with larger objects.

During object interactions, limited deformations of the contact interface also increase the difficulty of controlling object pose. With a small range for tolerating shear and torques, objects are much more likely to slip from contact, as interactions with the object closely resemble rigid body interactions [22]. In contrast, a more deformable sensor surface increases the area of stiction with the target object and provides a larger margin of error for robot manipulators through passive compliance, while also allowing a greater range of shear or torque before slip occurs.

Although larger contact patches and deformations are highly desirable, they introduce some new challenges. Because the sensing membrane is compliant, deformation occurs beyond the contact patch with the object. It can be difficult to accurately detect which parts of the membrane are in contact with the object exclusively from sensing the membrane’s deformation. The soft materials used to fabricate these compliant sensing surfaces have highly nonlinear mechanical properties that are difficult to model accurately and compute in real time for larger deformations.

In this work, we propose a contact patch segmentation algorithm that fuses proximity point clouds and tactile point clouds to detect contact patches of objects in extreme deformations of the sensing membrane. This algorithm leverages the multimodality of a large-scale proximity and visuotactile sensor enabled by a novel selectively transmissive soft membrane. The proximity depth modality is used to enhance tactile sensing functionality by providing essential object localization and geometry data during contact that is independent from the mechanical behavior of the soft membrane. With this key information and collocated proximity and tactile depth sensors, the intersection of the proximity and tactile point clouds provides the contact patch (Figure 1). We make three key contributions:

- 1) We present and evaluate our contact patch algorithm across low, medium, and high strain membrane states and against three baselines: proximity-only, tactile-only, and a membrane mechanics model. To the best of our knowledge, this is the first contact patch segmentation algorithm that fuses a point cloud proximity modality with tactile sensing.
- 2) We introduce design and fabrication techniques for a multimodal proximity and visuotactile sensor enabled by a selectively transmissive soft membrane.
- 3) We demonstrate applications of our contact patch algorithm in four use cases: varied stiffness membranes, torque and shear-induced out-of-plane membrane deformation, closed loop control for whole body manipulation, and pose estimation.

II. RELATED WORK

A. Multimodal Proximity and Tactile Sensors

Multimodal proximity and tactile sensors have been primarily explored in the form of sensing skins or sensing modules covering a robot end effector [23]. These sensing skins and modules commonly use a MEMs-based approach to measure proximity, integrating time-of-flight distance sensors to provide single point measurements for pre-grasp object detection [24]–[26] or re-grasping reflexes [27], [28]. However, the form factor of these individual MEMs proximity sensors are bulky and have wiring requirements that do not scale well for higher spatial resolution sensing. The lack of higher spatial resolution tactile and proximity sensing from the MEMs chips approach can severely hinder higher-level perception tasks such as object recognition, object tracking, and contact patch estimation.

FingerVision [29] is one of the few proximity and visuotactile sensors that provide a proximity modality, by using stereo vision to observe a pattern on a clear elastomer. However, this design requires a fundamental compromise in the spatial resolutions of proximity and tactile modalities: adding denser features to the pattern for tactile sensing occludes the proximity vision, while a sparse pattern limits the tactile resolution.

See-Through-Your-Skin [30], [31] is another proximity and visuotactile sensor that provides a proximity modality by modulating the membrane transparency via the two-way mirror effect with a semi-reflective surface. However, only one modality can be active at a time due to the transparency modulation: either proximity or tactile, but not both. Additionally, the two-way mirror sensing mechanism is not functional in high deformations, as the semi-reflective surface lets in too much external light and the sensor would be limited to the proximity modality.

Protac [32] is a proximity and visuotactile sensor that uses an electrically-controlled transparency-modulated film to switch between the tactile and proximity modalities. This approach, however, faces limitations in time resolution: the modalities are not synchronous and it takes 0.3s to switch between the modalities, which is a significant delay for real-time object interactions.

In this work, we overcome these limitations by using a selectively transmissive soft membrane [33], which blocks visible light and allows infrared light to pass through. We use an infrared time-of-flight depth camera to see through the membrane for the proximity modality, and a stereo RGB camera to sense the membrane for the tactile modality. Because the modalities do not interfere with each other, we achieve time-synchronous and simultaneous proximity and tactile point clouds.

B. Contact Patch Estimation

Contact patch estimation is an important functionality for tactile sensors, often the first step in processing tactile data for downstream tasks like pose estimation, estimating contact force distributions and direction, and object classification. The three main approaches to contact patch estimation for soft tactile sensors with hyperelastic materials are to apply

a threshold, use data-driven techniques to predict the contact patch, or solve a finite element method (FEM) model online.

Applying a threshold to displacement values to estimate the contact patch is the simplest and fastest method [22]. Typically a hand-selected number is used as the threshold and membrane displacement beyond the threshold is considered as part of the contact patch estimate. However, thresholds require manual tuning and do not generalize well across a large range of deformations.

Machine learning methods have been proposed to predict the contact patch but this approach brings another set of significant challenges: (1) the ability to generalize to a diverse set of object geometries, and (2) the laborious process of generating experimental datasets and an associated ground truth. Because the displacement to force mapping is dependent on object geometry, the datasets would have to be overwhelmingly extensive to capture a fraction of possible objects that could be encountered by the sensor. Additionally, the ground truth for each image would have to be generated by a corresponding FEM simulation [34], [35], for which accuracy scales with computation cost.

With the FEM approach, each element of the elastomer is typically modelled as a hyperelastic material, for which the stress-strain relationship is derived from a strain energy density function [36]. Commonly used hyperelastic models for elastomers include the Neo-Hookean, Ogden, and Mooney-Rivlin formulations. However, to determine the stress-stretch curves necessary to use these models, samples of the material must be tested in uniaxial tension, pure shear, and equibiaxial tension [37]. Collecting this type of data requires specialized equipment and does not generalize well across manufacturing variabilities in different samples. Most significantly, FEM approaches are very computationally expensive and do not run in real-time. Linear approximations or assumptions of a constant stiffness matrix can be made to speed up runtime [38], [39], but these assumptions do not hold in cases of extreme deformations.

III. SENSOR SYSTEM OVERVIEW

The design and fabrication of the sensor builds upon [33]. The sensor provides synchronized 640x480 px depth maps in both the proximity and tactile modalities at 30 Hz. The soft sensing surface is 355 mm x 205 mm and allows up to 85 mm of vertical displacement from a deflated membrane, before reaching the minimum sensing distances of the internal cameras. The sensor can be pressurized to inflate the membrane; the inflated height directly corresponds to how much the membrane can be vertically displaced. The proximity depth range extends approximately 100 mm beyond the membrane.

A. Selectively Transmissive Soft Membrane

We designed the new membrane presented in this work to achieve the following:

- 1) Provide a rich set of dense and random features in visible wavelengths (400 nm - 700 nm) to the internal stereo RGB camera for tactile point clouds.

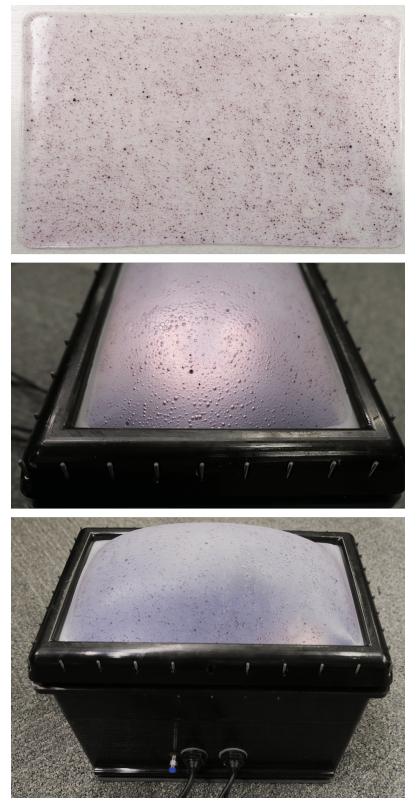


Fig. 2. Photos of the selectively transmissive soft membrane (top) and integration with the sensor system (middle and bottom).

- 2) Allow the infrared light (860 nm) emitted by the internal time-of-flight camera to pass through for the proximity point cloud.
- 3) Be produced from a simple, nontoxic fabrication process that facilitates easy repairs.

The soft membrane consists of two layers of silicone elastomer. The first layer is fully cured prior to pouring the next layer directly on top. The base elastomer is Ecoflex 00-35 Fast (Smooth-On), which we observe to have similar optical properties to Ecoflex 00-30 (Smooth-On) that has an attenuation of approximately 10db/cm at 860nm [40]. With the final thickness of the membrane at 1 mm, the membrane transmits approximately 90% of the emitted infrared (IR) light from the depth camera. In case of any small punctures or rips, the membrane can be quickly repaired by pouring another thin layer of the same silicone directly at the location of damage with no impact to sensing functionality.

The first layer consists of an IR-transparent, visibly-colored aqueous dye solution (VIS691A; QCR Solutions Corp, 0.1g/100mL concentration) hand-stirred with Ecoflex 00-35 Fast at a ratio of 1:10 (mL) dye to elastomer ratio. For the membrane in this work, we use 100 g of elastomer and 10 mL of dye solution. The dye solution is insoluble in silicone, which enables the formation of randomly encapsulated dye droplets to create the necessary visual pattern for depth estimation by the stereo RGB camera. The size of the dye droplets can be partially controlled by the amount of time spent mixing the dye and elastomer together; more time spent mixing is

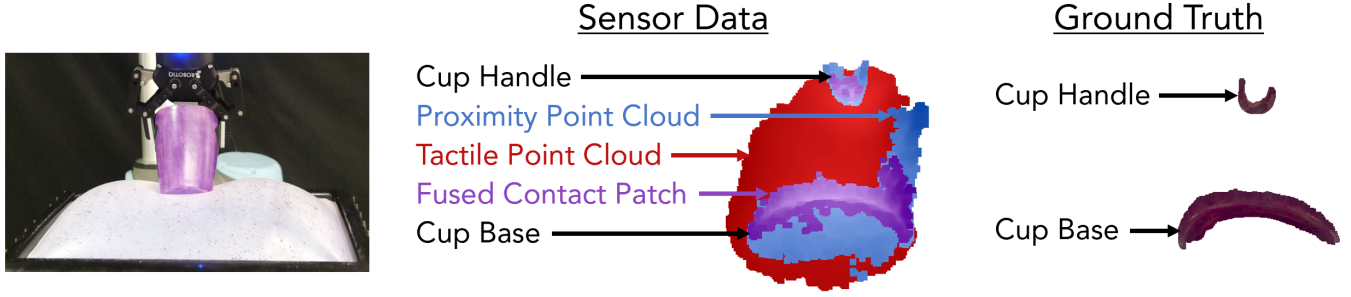


Fig. 3. The cup with a handle is pressed into the sensing surface of the multimodal visuotactile and proximity sensor by a robot arm. The corresponding sensing data is shown in the middle, where the contact patch estimation is computed by fusing the proximity and tactile point clouds. The ground truth contact patch is shown on the right.

correlated with smaller dye droplets. The desired size of the dye droplets is around 1-3 mm; this is large enough for the RGB stereo camera to detect, small enough for inconsequential stress concentrations introduced into the silicone elastomer, and creates a sufficient density of droplets for a rich visual pattern. Then, we mix 35 g of NOVOCS Matte (Smooth-On) with the dye and elastomer mixture. NOVOCS Matte imparts a matte finish on the membrane to reduce internal specular reflections and thins the elastomer mixture for even pouring into the mold. We pour the dyed elastomer into a laser-cut acrylic mold and let it fully cure at room temperature, which takes 5 minutes.

The final layer makes the membrane airtight by sealing any small pores in the membrane created by the encapsulated dye droplets, since the membrane will be inflated for use. We mix 30 g of Ecoflex 00-35 Fast with 20 g of NOVOCS Matte and pour it onto the first layer. The layer is then fully cured at room temperature in 5 minutes. For increased physical robustness, this final sealing layer can be increased in thickness at the cost of a decreased range of proximity sensing. For an increased range in proximity sensing, the silicone can be poured selectively (rather than an entire layer) on potential air leaks, which can be inferred by the locations of larger dye droplets.

B. Internal Electronics

The Intel Realsense L515, which has integrated RGB and time-of-flight (ToF) cameras, is used for proximity sensing. The IR light emitted by the L515 ToF camera travels through the membrane and does not sense the IR-transparent membrane itself. The Intel Realsense D405, a stereo RGB depth camera, is used for tactile sensing. Although the membrane is somewhat translucent, the visual texture of the membrane causes the D405 to produce a point cloud of the membrane only. The two cameras are placed immediately next to each other at the bottom center of the sensor. We design the active sensing region to be located where the FOVs of the D405's stereo depth and L515's ToF camera overlap; the entire exposed membrane is in view of both Realsense cameras. The cameras output data through USB-C ports, which are connected to an airtight USB-A 3.0 port that goes through the sensor housing. Both Realsense cameras are sampled

synchronously at 30 FPS, which is the fastest frame rate from the Realsense L515 ToF camera.

To provide internal lighting for the Realsense D405, we mount two LED ring lights to the sides of the sensor housing. Additionally, we include an internal air pressure sensor and a microcontroller that are also connected to the airtight USB-A port for data transmission. The internal air pressure sensor is required for the membrane mechanics model baseline comparison discussed in Section VC. An overview of the sensor system is shown in Figure 2.

C. Sensor Packaging

The sensor in this work is designed for integration into a whole-body robot manipulation system, so the sensing surface is scaled to cover the torso of the robot. The sensor can also be scaled down to be used as an end effector of a robot arm [33], though the size is limited by the minimum sensing distance of the L515's depth camera. The sensor housing is 3D printed (VeroBlack, J750, Stratasys) and consists of the main sensor chamber (403 mm x 280 mm x 284 mm) and lid (425 mm x 276 mm x 44 mm). The sensor chamber has rails compatible with 80/20 components for mounting to the robot body, as well as a push-to-connect tube fitting and two USB-A 3.0 ports. The lid features slots for M3 nuts and the chamber is attached with M3 screws. The lid clamps down on the membrane, sandwiched by two silicone gaskets, to form an airtight seal.

IV. PROXIMITY AND VISUOTACTILE FUSION FOR CONTACT PATCH ESTIMATION

The fusion algorithm outputs a point cloud of the estimated contact patch, which is constructed from the intersection of the set of points from the tactile and proximity point clouds shown in Figure 1 and Figure 3.

The data inputs to the algorithm are the proximity camera's RGB image, the proximity depth image, and the tactile depth image. The proximity camera's RGB image, which sees the membrane, is only used to remove noise from the proximity depth data. The proximity depth and tactile depth maps are used to compute the contact patch.

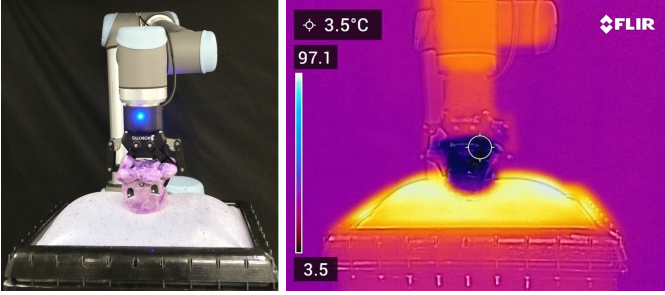


Fig. 4. The ground truth method for contact patch geometry exploits heat transfer between the object and sensor membrane at the contact interface. The object is painted with thermochromic paint that changes color when it comes into contact with the heated membrane.

1) *Frame Alignment*: First, the proximity RGB and tactile depth images are aligned to the proximity depth map. The proximity RGB and depth images are aligned using the Intel Realsense L515 intrinsics, since the depth and RGB cameras are located on the same device. The proximity depth and tactile depth images are aligned using a manually calibrated homography matrix.

2) *Proximity Pre-Processing*: Depending on the curvature of the inflated membrane, some areas of the membrane can be infrared reflective and produce noise in the proximity depth data. We convert the proximity RGB image to HSV and use manually tuned thresholds to create a mask that removes any pixels that match the color of the membrane when no objects are in contact or near the membrane surface. The mask is then applied to the proximity depth image, which filters out the internal reflections of the emitted infrared light.

3) *Contact Patch Estimation*: The contact patch is estimated by computing the intersection of the tactile and proximity depth images. We compute an intersection mask with a pixel-wise comparison of distance values from the tactile and proximity depth maps:

$$|d_p - d_t| \leq t|d_p|$$

where d_p is the proximity distance, d_t is the tactile distance, and t is the tolerance. If the difference in tactile and proximity distance values at a pixel satisfy the inequality, the pixel is considered a match and part of the contact patch. We manually tune the value of t to produce the contact patch that best matches ground truth, and we found that $t = 0.03$ works well; in our experiments, the tolerance distance values range from 6mm-8mm. The intersection mask is applied to the proximity depth image to produce the contact patch estimation. We use the proximity depth image instead of the tactile depth image because the proximity depth data is significantly more robust to inconsistent room lighting conditions. The contact patch depth image is then projected to a point cloud and we apply a statistical outlier rejection filter to remove any extraneous points before outputting the final contact patch point cloud estimation.

TABLE I
PARAMETERS FOR GROUND TRUTH METHOD.

Object	Membrane Temperature (Celsius)	Contact Time (s)
octopus	70	5.5
cup	100	9
cube	95	9

V. EXPERIMENTAL METHODS

A. Ground Truth

It has been challenging to provide an experimental ground truth method for contact patches because the contact patch is always occluded from external viewpoints and surface mounted sensors interfere with the object interaction. Thus, most works use simulation or model-based methods [35], [41], [42] to evaluate the contact patch estimation. However, our work targets scenarios when simulation or model-based methods fail, so we must use an experimental method for ground truth.

Our ground truth method leverages thermal conduction at the contact interface. Similar methods have been presented to annotate human grasps on objects by capturing heat transfer from human hands with either thermal cameras [43] or thermochromic paint [44] and RGB-D cameras.

The object dataset is painted with three coats of thermochromic paint (Elmers), which changes color from purple (cold) to pink (hot) with temperature. The objects are placed in a fridge and cooled to 3.5°C until the purple color is opaque and visually consistent, usually 15 minutes. Prior to running the experiment, the membrane is heated to temperatures ranging from 70°C-100°C with a heat gun. The precise temperature of the membrane and contact time is tuned per object to prevent noise from thermal radiation; the chosen temperature prevents color change when the object is within 1 mm of the membrane, but enables color change when contact occurs. The temperatures and contact time vary per object because each object has a different specific heat capacity, which governs the temperature at which the thermochromic paint changes color (Table I). We monitor the spatial uniformity of the membrane and object temperature with a FLIR thermal camera.

When the cooled object makes contact with the heated membrane, the thermochromic paint changes color where contact occurs. The object is then scanned with a high-resolution 3D scanner (Space Spider, Artec), with an accuracy of 0.05mm. The 3D scan of the object is then thresholded by color to determine the contact patch geometry.

We make the following two assumptions for this ground truth method:

- 1) Because all of the objects are relatively more rigid than the soft membrane, we assume that the object does not deform when contact occurs, so the scan of the object geometry is equivalent to the contact patch geometry.
- 2) This method captures the maximum contact patch, which we assume to occur when the membrane is at its highest deformation during its interaction with the object.

B. Membrane Strain Measurement

We use the following method to correlate displacement of the object into the membrane to 2D strain in the membrane (Figure 5). High strain in the membrane is difficult to simulate accurately due to its hyperelastic material properties and manufacturing imperfections, so we take an experimental approach to strain measurement.

First, we use a laser-cut stencil to pattern an IR and visibly opaque membrane with a uniform grid of dots with known spacing (10mm). This membrane is fabricated to have the same thickness and physical dimensions as the membrane described in Section IIIA. We use the Realsense L515 to capture an RGB-D point cloud of the patterned membrane as the robot arm applies a vertical displacement with an object from our object dataset. We measure the distances between the centroids of each dot on the patterned membrane from the point cloud, which is used to calculate the maximum in-plane strain along the length and width of the membrane. The calculated maximum strain is then used to find the vertical displacement required to impart the desired strain states for our experiments: low - 10%, medium - 60%, high - 100%.

C. Baselines

For the tactile-only and membrane mechanics model baselines, we use an unpatterned IR-opaque silicone membrane

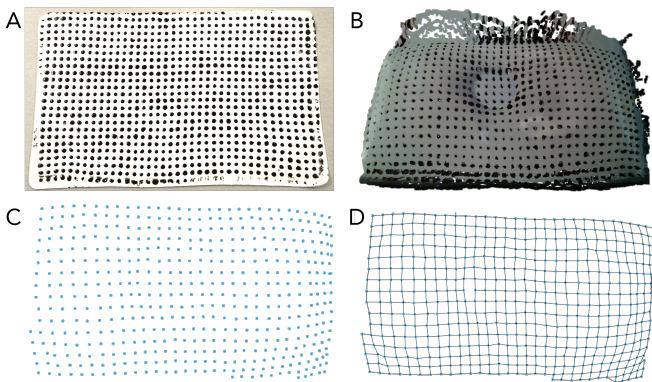


Fig. 5. Method used to calculate membrane strain. A) Uniform grid of dots with known spacing is patterned on the membrane. B) Object (octopus, not shown) is pressed into the membrane and the RGB-D point cloud is captured. C) The centroids of the dots from the RGB-D point cloud are isolated. D) The distances between the centroids are measured to calculate strain.



Fig. 6. This membrane is opaque to IR and visible light. It is used for the tactile-only and membrane mechanics model baselines.

TABLE II
COMPUTATION TIME FOR ONE FRAME OF A CONTACT PATCH ESTIMATION, USING AN INTEL CORE I7-8650U CPU.

Algorithm	Computation Time (s)
tactile-only (baseline)	0.03
proximity-only (baseline)	0.03
fusion (ours)	0.07
mechanics model (baseline)	0.3

with the same physical dimensions as the selectively transmissive membrane (Figure 6). We use the Realsense L515 ToF depth camera to collect data for both of these baselines, since using a ToF depth camera with this sensor system can replicate a closely related design [8] and fulfill the input requirement of ToF depth data for the membrane mechanics model. For the proximity-only baseline, we use the selectively transmissive membrane and the depth data from the Realsense L515 ToF camera. The computation times for each algorithm are shown in Table 2.

1) *Tactile-Only*: The tactile-only approach exclusively uses a tactile point cloud and a thresholding scheme to estimate the contact patch. In this work, the threshold is implemented as follows: the contact patch is identified as the highest 60% of deformed points on the membrane, compared to a reference point cloud of an inflated membrane with no object-induced deformation. We found that an absolute threshold approach (i.e., points below a certain distance), although common for less deformable visuotactile sensors, gives much worse contact patch estimations and would not be a realistic baseline.

2) *Proximity-Only*: The proximity-only approach exclusively uses the proximity point cloud. This baseline uses a reference point cloud of the inflated membrane with no object-induced deformation. The contact patch is estimated as any points that are closer to the camera than the reference point cloud.

3) *Membrane Mechanics Model*: We use the first principles continuum mechanics model presented in [39] as a baseline. The model predicts the linear elastic deformation of a mesh of the membrane given the pose and geometry of a rigid object in contact with the sensor. Then, the model is used to solve the inverse problem of estimating the contact patch based on tactile depth and internal air pressure data from the sensor, using a sparse convex Quadratic Program formulation for real-time solutions. The model assumes that the contact surface is frictionless, deforms linearly, and does not wrinkle or fold.

VI. EVALUATION

To evaluate our proposed algorithm, we measure the accuracy of the geometry of the estimated contact patch when the membrane is in low (approx. 10%), medium (approx. 60%), and high (approx. 100%+) strain states. We use a dataset of three objects: a stuffed octopus, a Rubiks cube, and a cup. These objects were chosen to represent a diverse set of geometries: edges (Rubiks cube), curves (octopus), and non-convex contacts (cup). Each object is grasped by a Robotiq gripper mounted to a UR10 robot arm and pushed into the sensor. The vertical displacement of each trial is determined by what is needed to induce the desired strain in the membrane.

We compare our results to ground truth and three baselines: tactile-only, proximity-only, and the mechanics model-based method. The metric for geometric accuracy of the contact patch point clouds is root mean squared error (RMSE) of the estimated contact patch point cloud and the ground truth point cloud after manual alignment. For the membrane mechanics model-based method, we crop the estimated contact patch to exclude the outer edges of the sensor interface since the model cannot consistently predict the “bulging” behavior of the membrane, leading to spurious estimated contacts detected there. The resulting contact patch estimations are shown in Figure 7 and the RMSE analysis per strain state is shown in Figure 8.

A. Low Strain Experiments

We induce low strain in the membrane by commanding the UR10 robot arm to press the object 4 mm into the membrane. The initial maximum height of the membrane is 314 mm from the internal cameras at the base of the sensor.

For the octopus, the contact patch estimation from the fusion algorithm has the lowest RMSE (Figure 8). Visually, the geometry of the contact patch estimated by the fusion algorithm also best matches the geometry of the ground truth patch (Figure 7). The proximity-only algorithm overestimates the contact patch. The overestimation of the contact patch is because the proximity-only algorithm does not consider the behavior of the membrane after contact, so it is unable to estimate where the object is actually in contact with the membrane. However, the geometry of the contact patch is still quite accurate because the proximity modality can measure the object geometry accurately. The tactile-only algorithm underestimates the contact patch, likely because the threshold is not specifically tuned to this strain range. At a low strain range, the threshold should be increased to capture more of the deformed points, since more of the membrane deformation can be attributed to the contact itself. However, increasing this threshold number may not generalize well to higher strain states, as the membrane starts to deform beyond the object’s contact patch. The membrane mechanics model estimates a very small patch, with the geometry of the patch largely dictated by the triangular elements of the mesh.

The fusion algorithm also performed the best compared to the baseline methods for the cup with handle, with separate multiple contacts. Some noise from IR reflections on the surface of the membrane was not completely eliminated by the RGB masking in the proximity modality, resulting in an extraneous contact patch detected. Using the tactile sensing modality helped make the extraneous contact patch smaller, but did not completely remove it because of the imperfect height alignment of the internal depth cameras and the tolerance used to compute the intersection of the point clouds. The extraneous contact patch is much more prominent in the proximity modality, which produced the third-best estimation of the contact. The estimated contact from tactile sensing is the second-best estimation. Compared to ground truth, it is difficult to visually distinguish which parts of the estimated patch are actually in contact with the cup, due to the noise from

the membrane deformation propagating beyond the contact patch. The membrane mechanics model failed to produce an estimate of the contact patch, because the deformation is within the same magnitude as the simulated depth camera noise and thus indistinguishable.

With the cube, the tactile-only, proximity-only, and fusion algorithms all performed similarly and very well, with RMSEs less than 2 mm and within 16% of each other. The flat, planar face of the cube produces a large and dense contact patch with the membrane and the edges of the cube are captured very well with the proximity-only and fusion algorithms. In comparison, the tactile-only contact patch has significantly more noise around the border of the cube. The membrane mechanics model failed to estimate the contact patch, for the same reason as the cup.

B. Medium Strain Experiments

We program the robot arm to press the object 24 mm into the membrane for the membrane’s medium strain state. Similar to the low strain experiments, the initial maximum height of the membrane is 314 mm.

For the octopus, the fusion algorithm had the best performance compared to the baselines. Similar to the estimations in the low strain experiment, the proximity-only baseline overestimated the contact patch while the tactile-only baseline underestimated the contact patch. Compared to the tactile-only baseline, the proximity-only baseline and fusion algorithm better captured the geometry of the outline of the ground truth contact patch. The membrane mechanics model greatly underestimated the contact patch, with the overall geometry of the patch dictated by the coarse mesh of the membrane - the triangular edges are clearly seen in the geometry of the contact patch estimation.

For the cup, the fusion algorithm clearly best estimates the contact patch. Here, the advantages of the fusion approach is most clearly demonstrated: the tactile-only baseline is not able to distinguish two different contacts from the edge of the cup and the handle, while the proximity-only baseline estimates significant extraneous contact along the side of the cup near the handle. However, the fusion algorithm clearly distinguishes the two contacts while avoiding the same overestimation as proximity. Similar to the octopus, the membrane model estimation is again dominated by the geometry of the coarse mesh of the membrane, and also is unable to distinguish two different contact points of the cup base and handle. Like in the small strain case, it is also possible that the deformation from the cup handle is within the same magnitude as the simulated depth camera noise and the mechanics model failed to produce an estimate of the cup handle contact.

With the cube, the tactile-only baseline and fusion algorithms both produced similarly accurate estimates of the contact patch. The proximity-only baseline greatly overestimates the contact patch, estimating substantial contact along the sides of the cube. The mechanics model significantly underestimates the size of the contact patch, but is able to roughly capture the square geometry of the cube.

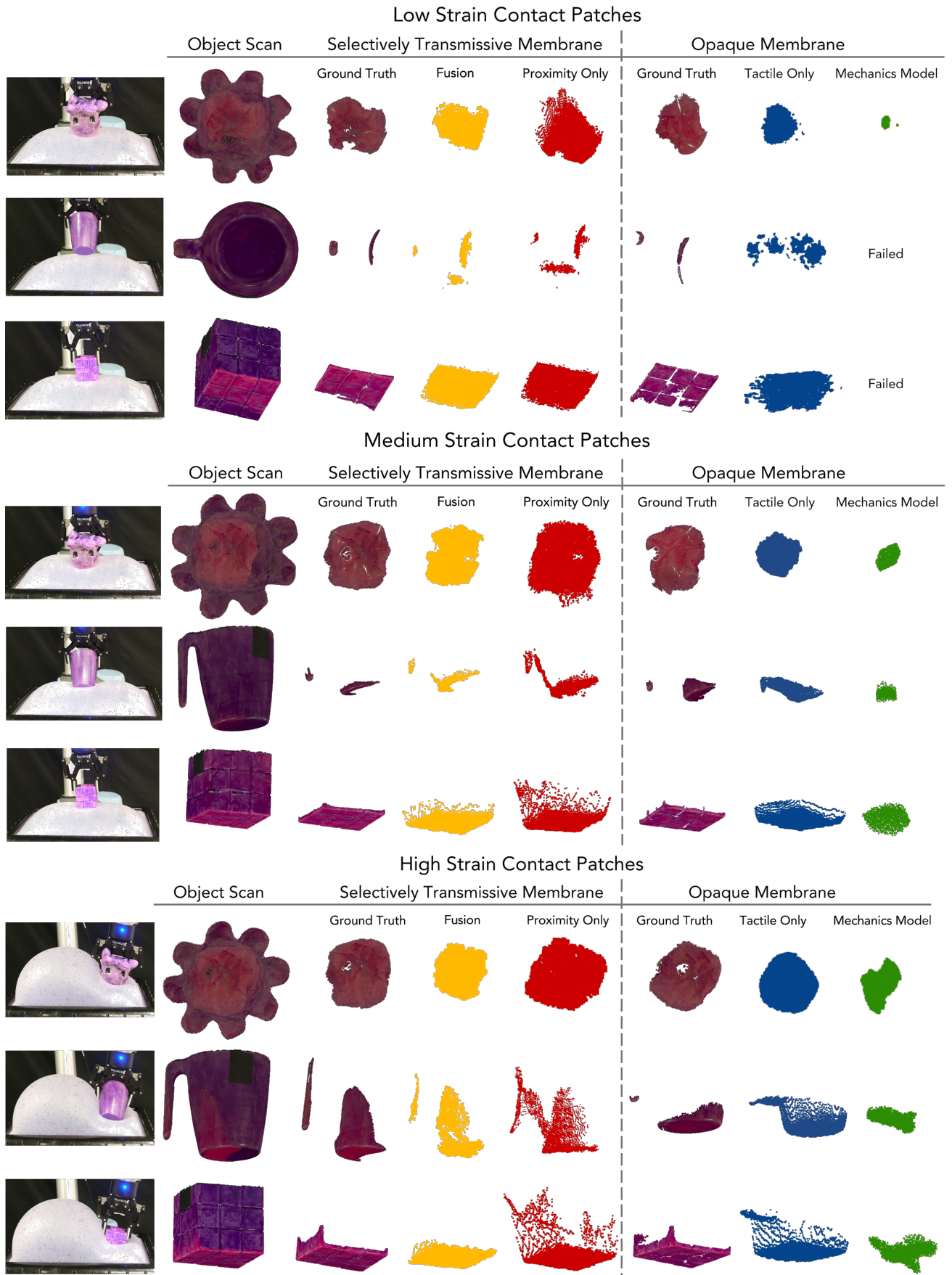


Fig. 7. Visualizations of the estimated contact patch across low, medium, and high strain states of the membrane. Our proposed algorithm, Fusion, fuses the visuotactile and proximity modalities of the sensor enabled by the selectively transmissive membrane. The baselines for comparison are Proximity Only, Tactile Only, and Mechanics Model. The ground truth is a color-segmented 3D scan of the object, where pink designates contact.

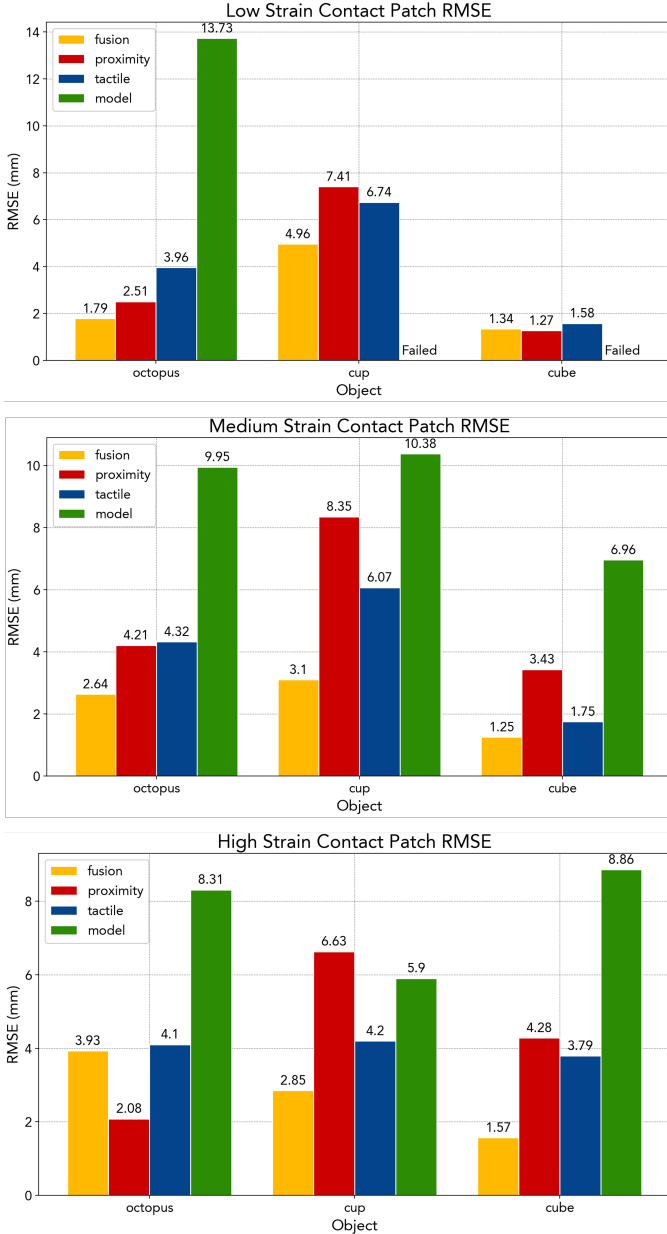


Fig. 8. RMSE for the contact patch point clouds estimated by the fusion (ours), proximity only, tactile only, and membrane mechanics model algorithms per object. Lower RMSE is better.

C. High Strain Experiments

The membrane is inflated to have an initial maximum height of 380 mm. The UR10 robot arm presses the object 120 mm into the membrane to produce the high strain state of the membrane. The object was pressed off-center into the membrane to allow the uncontacted region to expand outwards and produce high strains in the membrane.

The proximity-only baseline provided the most accurate contact patch for the octopus, despite slightly overestimating the size of the patch. The fusion and tactile-only baseline performed very similarly and both underestimated the patch. The mechanics model did produce a patch estimate but did not capture the circular geometry of the object well, estimating distinct corners along the edges of the patch.

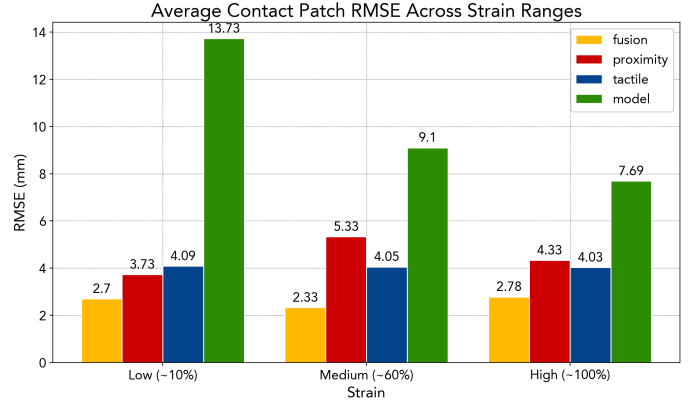


Fig. 9. Average RMSE for the contact patch point clouds estimated by the fusion (ours), proximity only, tactile only, and membrane mechanics model algorithms per strain state. Lower RMSE is better.

For the cup, the fusion algorithm again excels capturing the two distinctive contact patches from the base of the cup and the handle. The proximity-only baseline greatly overestimates the contact patch, with more noticeable error along the sides of the cup. The mechanics model significantly underestimates the contact patch and is not able to distinguish the contact from the handle of the cup. The tactile-only baseline is not able to distinguish separate contacts between the handle and the base of the cup. In this case, because the cup is pressed off-center into the membrane, the tactile-only threshold approach shows significant bias in overestimating contact in the area of the membrane that undergoes high strain as it bulges towards the center. Because the threshold approach is only based on identifying total deformation, it will always be biased towards estimating false contacts along areas of high strain, even if contact did not occur.

The proximity-only and tactile-only baseline contact estimations for the cube also show the same limitations of thresholding in an off-center contact case, and overestimate contact in areas where the membrane is experiencing high strain. We note that the proximity-only estimation of the cube likely includes noise from IR light reflecting off the membrane on the right, since it is impossible to see two sides of a cube simultaneously. The fusion algorithm produces the most accurate estimation, although it underestimates the amount of contact along the side of the cube that is closest to the center of the sensor. The mechanics model does produce a contact patch estimate in approximately the correct location, but it does not resemble the geometry of the contact patch.

D. Discussion

Although our proposed fusion algorithm is simple, it generalizes well across our object dataset and strain range, outperforming all of the baselines on average (Figure 7). Fusing both the tactile and proximity modalities is key to overcoming the shortcomings of each modality: the proximity modality tends to overestimate contact while tactile thresholding tends to underestimate contact. There are only two specific cases where a baseline has a lower RMSE than the fused contact patch: the proximity-only estimations in the high-strain octopus contact

Complex Membrane Mechanics

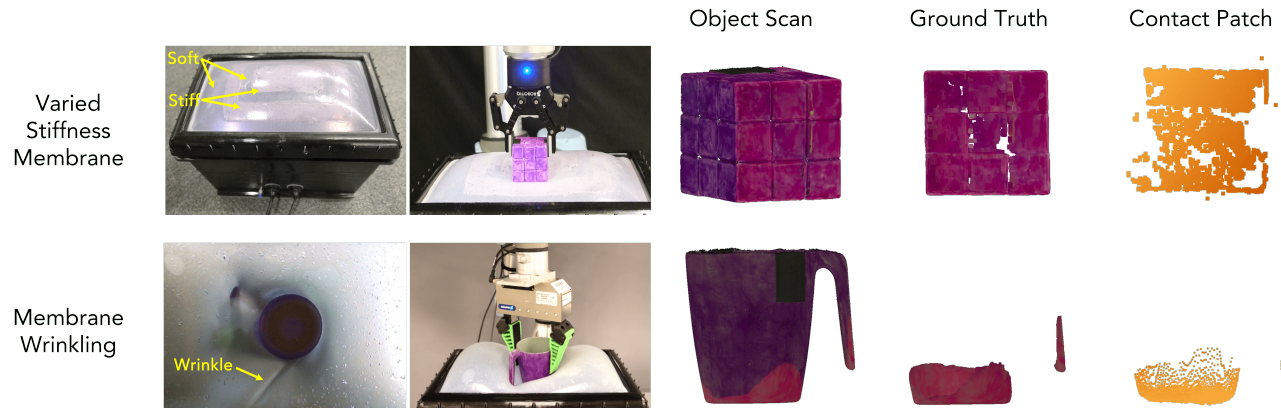


Fig. 10. We demonstrate the proposed fusion algorithm for contact patch estimation in two applications with complex membrane mechanics: a varied stiffness membrane (top) and membrane wrinkles (bottom).

patch and the low-strain cube patch. With both of these cases, the proximity-only baseline overestimation of the contact patch better captured the ground-truth contact patch geometry than the underestimation from the fusion algorithm. In all other cases, the fusion algorithm consistently produced the most accurate contact patch with the lowest RMSE error.

VII. DEMONSTRATIONS

We demonstrate several applications of the contact patch fusion algorithm to highlight the usefulness of fast and accurate contact patch estimation during complex membrane deformations: varied stiffness membranes, torque and shear-induced membrane wrinkling, closed loop control, and pose estimation.

A. Complex Membrane Mechanics

1) *Varied Stiffness Membranes*: Spatially varied stiffness patterns can be used to program complex 3D shapes [45], [46] that could be tailored towards manipulation tasks, such as directing the inflation of the membrane to a flatter shape for larger contact areas with less force, rather than a uniform and curved expansion of the membrane. Additionally, actively controlled variable stiffness materials [47], [48] are a rich area of soft robotics research and could potentially be used to change the stiffnesses and shapes of robot end effectors to suit different tasks in real time. Because the selectively transmissive membrane exclusively relies on optical properties to enable the tactile and proximity modalities, the stiffness of the membrane can be varied with no impact to the sensing functionality. This sensing approach, used in conjunction with the mechanics-independent proximity and tactile fusion contact patch algorithm, enables contact patch estimation for arbitrary patterns of varied stiffness in the sensing membrane.

In this demonstration, we achieve varied stiffness by using two different base silicone elastomers with different Shore hardnesses (Figure 8). The stiff and soft silicones are cured together to form one cohesive varied stiffness membrane. The two stiff regions are made from a stiffer silicone, Dragonskin

10 Fast (Smooth-On), which has a Shore hardness of 10A. The two soft regions are made from Ecoflex 00-35 Fast (Smooth-On), which has a Shore hardness of 00-35. Dragonskin 10 is approximately 8x harder than Ecoflex 00-35. The same fabrication method presented in Section IIIA is used to produce the varied stiffness membrane, albeit with the above specified base elastomers.

Here, the advantage of our approach is the ease-of-use across many different stiffness patterns and potentially actively controlled variable stiffness membranes. The proximity-only and tactile-only baseline methods would require tuning for each membrane pattern due to the variance of inflated shapes. The membrane mechanics model would require generating a new mesh that matches both the stiffness pattern and mechanical properties of the different membrane patterns. A machine learning approach would require more data for each new membrane pattern.

We run the medium strain cube experiment with the varied stiffness membrane. The estimated contact patch is shown in Figure 8. Compared to ground truth, the RMSE of the estimated contact patch is 1.09 mm.

2) *Torque and Shear-Induced Wrinkling*: A highly deformable contact interface that tolerates a large range of shear and torque before slipping is key to maintaining stiction with a target object. This feature can be critical in mitigating errors in robot manipulators by reducing the requirement for precise perception and control during a task, or simplifying planning by minimizing regrasp or repositioning the object. However, these torques and shear forces can create wrinkles in the deformable membrane surface, which are very difficult to model even with computationally expensive FEM approaches. In this demonstration, we highlight the advantage of our mechanics-independent, fusion contact patch algorithm to estimate the contact patch of a cup while the membrane is wrinkled. The robot arm presses the cup into the surface of the sensor and rotates it 45° , creating wrinkles behind the cup handle and along the sides of the cup. The estimated contact patch is shown in Figure 8. In comparison with ground truth, the RMSE of the estimated contact patch is 3.49 mm. The

geometry of the contact patch qualitatively matches well with ground truth, accurately capturing the side of the cup handle that is in contact with the membrane despite the wrinkles.

B. Closed-Loop Control for Whole-Body Manipulation

We demonstrate the real-time speed and integration of the proximity and tactile fusion algorithm with a closed-loop controller and physical robot system for a whole body manipulation task: balancing a stack of books (Figure 9). The robot system, Punyo-1 [49], consists of the visuotactile and proximity sensor placed on the robot’s torso, a Kinova Jaco robot arm on each side of the sensor with soft padding, and a Puget computer. An empty cardboard tray is held by Punyo-1 and pressed into the sensorized torso. As each book is placed on the tray held by the robot, the tray’s center of mass changes and the robot adjusts the roll angle of the tray to balance the books. The angle of the tray of books is sensed with the proximity and visuotactile fusion contact patch algorithm.

The sensor runs at 30 FPS and the contact patch is calculated for each frame. To calculate the angle of the tray, we use principal component analysis (PCA) on the contact patch. We found that PCA of the contact patch gives less noisy estimations of the tray position compared to the proximity-only modality, which has added noise from sensing the books. The estimated angle of the tray is then given to the whole-body

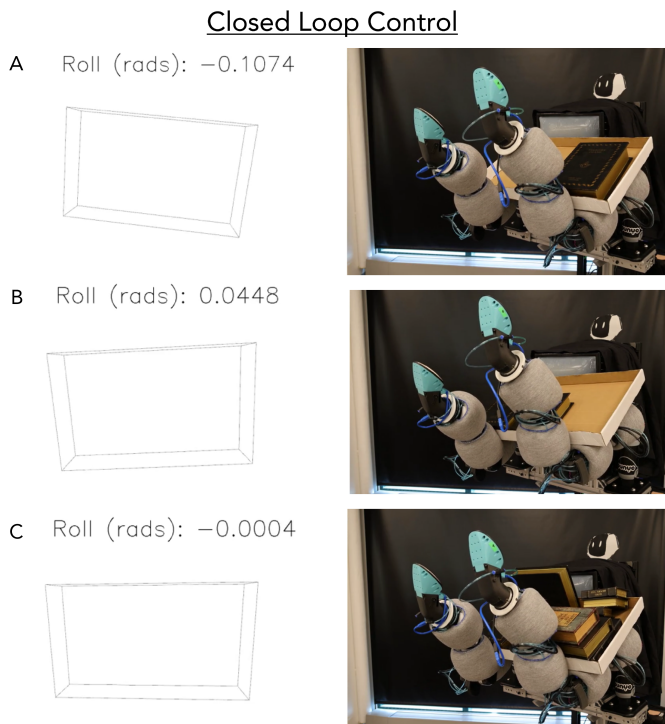


Fig. 11. The sensor is integrated on a dual arm robot platform as the chest of the robot. The sensor estimates the angle from the contact patch of the tray of books in order to balance the tray as more books are added. This task demonstrates the real-time speed and integration of the proximity and tactile fusion algorithm with a closed-loop controller. A) The tray tilts towards the right with the weight of the book. B) The tray tilts towards the left as the book slides towards the left. C) The robot holds the tray level to balance the stack of books.

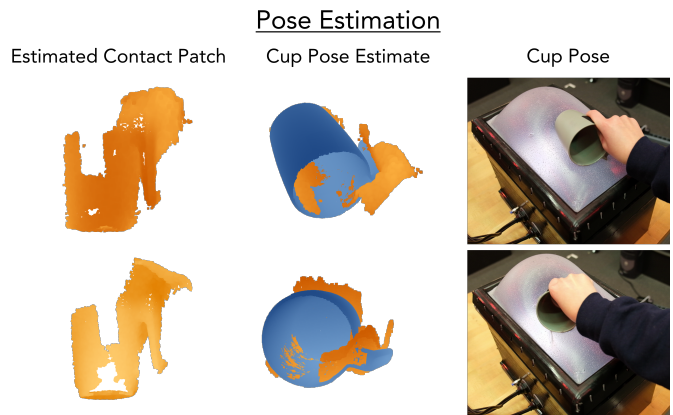


Fig. 12. The cup simultaneously rotates about the handle and translates across the membrane. The pose estimate from the contact patch qualitatively matches very well. The estimated contact patch has an atypical amount of noise near the top of the cup, which comes from the proximity estimation of the hand, due to adverse lighting conditions.

PD controller at a frequency of 29 Hz. We use two arm motion primitives to adjust the angle of the tray.

C. Pose Estimation

In this demonstration, we show that our contact patches are compatible with a standard pose estimation pipeline. Because our contact patch algorithm provides accurate contact patches in high deformation of the membrane, the greater conformal contact allows for large and dense contact patch point clouds that are easy to use with a standard Iterative Closest Point (ICP) implementation from Open3D [50] to estimate pose. Exclusively using contact patches for pose estimation, rather than only the proximity modality, could be advantageous in cluttered environments where an additional segmentation step would be necessary to isolate the object of interest. We estimate the pose of a cup for 5 s as the cup simultaneously rotates about the handle and translates across the sensor surface. Because of stiction between the cup and the sensor surface, wrinkles are created in the membrane during the cup trajectory. We assume a known model of the cup geometry. In the first frame of the trajectory, the cup is manually registered to the estimated contact patch. For the following frames that measure the rest of the trajectory, the relative transformation of the cup is estimated for each timestep.

We observe that the key feature of the cup that leads to stable pose estimations is visibility of the handle in the contact patch. The pose estimation tends to become unstable when the handle is not observable and when there are fewer points in the contact patch estimation. Qualitatively, the pose estimate of the cup matches very well (Figure 10) and is fairly stable across the 5 s of data. Because the external environment was significantly brighter than the internal sensor chamber in this experiment, the tactile depth camera struggled to accurately estimate the membrane point cloud, leading to noise in the contact patch from the proximity depth sensing the hand holding the cup. The sensor could be modified to increase robustness to external light by increasing the intensity of the

internal LEDs in the sensor chamber and formulating a more visibly-opaque membrane by adding more dye.

A future application of this work could be tactile SLAM for simultaneous object pose estimation and reconstruction [51], [52].

VIII. CONCLUSION AND FUTURE WORK

In this study, we introduced a proximity and visuotactile point cloud fusion algorithm to detect contact patches with soft membranes across an unprecedented range and type of deformation. The key idea of the algorithm is that the contact patch can be identified as the set of points where the proximity point cloud and tactile point cloud intersect. Because the proximity point cloud provides localization and a point cloud of the object geometry independent of membrane mechanics, our method is not limited by the difficulties of accurately modeling the complex deformations in hyperelastic membrane materials that occur during real-world object interactions. This is not possible for visuotactile sensors that rely exclusively on the tactile modality.

We also presented the design and fabrication techniques for a selectively transmissive soft membrane that enables the dual sensing modalities. The formulation of the soft membrane leverages the insolubility of a visibly-colored, IR-transparent aqueous dye solution in a highly elastic silicone elastomer to create visual texture for tactile sensing with a stereo RGB depth camera and enable proximity sensing for an internal ToF depth camera. The fundamental sensing mechanism of selective light transmission is robust to manufacturing variances in the membrane, so the proposed sensor fusion algorithm requires no tuning for different batches of membranes. Additionally, the fabrication process uses accessible, off-the-shelf materials and produces a physically resilient and easily repairable sensing interface.

Furthermore, we conducted an extensive study of the accuracy of contact patch geometry for a diverse object dataset across three regimes of deformation: low strain, medium strain, and high strain. We found that the proposed proximity and visuotactile fusion algorithm used with the selectively transmissive membrane had the best performance across all three strain categories.

We demonstrated the use of this sensor and algorithm with three applications: use cases with complex membrane mechanics, closed loop control for balancing a stack of books with a dual arm manipulation platform, and pose estimation.

Moving forward, we would like to explore modifying the sensor design to achieve higher sampling frequencies for more dynamic manipulation tasks. The current sensor is limited by the frame rate of the proximity ToF depth camera, to maintain synchronous sampling with the tactile stereo RGB depth camera. The selective transmission sensing mechanism does not solely rely on using a ToF depth camera; the requirement is for an IR camera. A high-speed IR camera (stereo or mono) could be used to replace the ToF depth camera to increase the speed of the entire sensing system.

This work could also be extended by using this contact patch algorithm and selective light transmission sensing mechanism

for variable stiffness surfaces. As the soft robotics field moves towards multifunctional materials with tighter integration of soft sensors and actuators, a natural next step for this work could be integration with an actuating surface that changes stiffness and shape in real-time to manipulate objects.

Another future direction for this work is to further investigate the use of proximity depth sensing in perception for manipulation. In this paper, we presented proximity as a modality to support and enhance tactile sensing functionality. It would be interesting to study the benefits of proximity sensing as a more independent modality in a manipulation pipeline that incorporates vision and tactile sensing.

ACKNOWLEDGMENT

The authors would like to thank the PrOps team, Aimee Goncalves, Dr. Jose Barrios, Dr. Aykut Önel, Eric Cousineau, and Alex Alspach at the Toyota Research Institute for helpful discussions, assistance with setting up experiments, and hardware design advice. The authors are grateful for assistance with running experiments and insightful discussions about the pose estimation demonstration from William Yang at the University of Pennsylvania. The authors also thank Gregory Campbell from the University of Pennsylvania for assistance with running experiments.

REFERENCES

- [1] Chunfeng Wang, Lin Dong, Dengfeng Peng, et al. “Tactile sensors for advanced intelligent systems”. In: *Advanced Intelligent Systems* 1.8 (2019), p. 1900090.
- [2] Kazuhiro Shimonomura. “Tactile image sensors employing camera: A review”. In: *Sensors* 19.18 (2019), p. 3933.
- [3] Benjamin Shih, Dylan Shah, Jinxing Li, et al. “Electronic skins and machine learning for intelligent soft robots”. In: *Science Robotics* 5.41 (2020), eaaz9239.
- [4] Wenzhen Yuan, Siyuan Dong, and Edward H Adelson. “Gelsight: High-resolution robot tactile sensors for estimating geometry and force”. In: *Sensors* 17.12 (2017), p. 2762.
- [5] Akhil Padmanabha, Frederik Ebert, Stephen Tian, et al. “Omnitact: A multi-directional high-resolution touch sensor”. In: *2020 IEEE International Conference on Robotics and Automation (ICRA)*. IEEE. 2020, pp. 618–624.
- [6] Won Kyung Do and Monroe Kennedy. “DenseTact: Optical tactile sensor for dense shape reconstruction”. In: *2022 International Conference on Robotics and Automation (ICRA)*. IEEE. 2022, pp. 6188–6194.
- [7] Nathan F Lepora. “Soft biomimetic optical tactile sensing with the TacTip: A review”. In: *IEEE Sensors Journal* 21.19 (2021), pp. 21131–21143.
- [8] Alex Alspach, Kunimatsu Hashimoto, Naveen Kuppuswamy, et al. “Soft-bubble: A highly compliant dense geometry tactile sensor for robot manipulation”. In: *2019 2nd IEEE International Conference on Soft Robotics (RoboSoft)*. IEEE. 2019, pp. 597–604.

- [9] Mike Lambeta, Po-Wei Chou, Stephen Tian, et al. “Digit: A novel design for a low-cost compact high-resolution tactile sensor with application to in-hand manipulation”. In: *IEEE Robotics and Automation Letters* 5.3 (2020), pp. 3838–3845.
- [10] Yipai Du, Guanlan Zhang, and Michael Yu Wang. “3D Contact Point Cloud Reconstruction From Vision-Based Tactile Flow”. In: *IEEE Robotics and Automation Letters* 7.4 (2022), pp. 12177–12184.
- [11] Yazhan Zhang, Zicheng Kan, Yu Alexander Tse, et al. “Fingervision tactile sensor design and slip detection using convolutional lstm network”. In: *arXiv preprint arXiv:1810.02653* (2018).
- [12] Mingxuan Li, Lunwei Zhang, Tiemin Li, et al. “Continuous Marker Patterns for Representing Contact Information in Vision-Based Tactile Sensor: Principle, Algorithm, and Verification”. In: *IEEE Transactions on Instrumentation and Measurement* 71 (2022), pp. 1–12.
- [13] Mingxuan Li, Tiemin Li, and Yao Jiang. “Marker Displacement Method Used in Vision-Based Tactile Sensors—From 2D to 3D-A Review”. In: *IEEE Sensors Journal* (2023).
- [14] Ian H Taylor, Siyuan Dong, and Alberto Rodriguez. “GelSlim 3.0: High-resolution measurement of shape, force and slip in a compact tactile-sensing finger”. In: *2022 International Conference on Robotics and Automation (ICRA)*. IEEE. 2022, pp. 10781–10787.
- [15] Megha H Tippur and Edward H Adelson. “GelSight360: An Omnidirectional Camera-Based Tactile Sensor for Dexterous Robotic Manipulation”. In: *2023 IEEE International Conference on Soft Robotics (RoboSoft)*. IEEE. 2023, pp. 1–8.
- [16] Chaofan Zhang, Shaowei Cui, Shuo Wang, et al. “High-Precision 3D Reconstruction Study with Emphasis on Refractive Calibration of GelStereo-Type Sensors”. In: *Sensors* 23.5 (2023), p. 2675.
- [17] Sudharshan Suresh, Zilin Si, Joshua G Mangelson, et al. “ShapeMap 3-D: Efficient shape mapping through dense touch and vision”. In: *2022 International Conference on Robotics and Automation (ICRA)*. IEEE. 2022, pp. 7073–7080.
- [18] Maria Bauza, Antonia Bronars, and Alberto Rodriguez. “Tac2pose: Tactile object pose estimation from the first touch”. In: *arXiv preprint arXiv:2204.11701* (2022).
- [19] Sudharshan Suresh, Zilin Si, Stuart Anderson, et al. “MidasTouch: Monte-Carlo inference over distributions across sliding touch”. In: *Conference on Robot Learning*. PMLR. 2023, pp. 319–331.
- [20] Yuan Gao, Shogo Matsuoka, Weiwei Wan, et al. “In-Hand Pose Estimation Using Hand-Mounted RGB Cameras and Visuotactile Sensors”. In: *IEEE Access* 11 (2023), pp. 17218–17232.
- [21] Gregory Izatt, Geronimo Mirano, Edward Adelson, et al. “Tracking objects with point clouds from vision and touch”. In: *2017 IEEE International Conference on Robotics and Automation (ICRA)*. IEEE. 2017, pp. 4000–4007.
- [22] Miquel Oller, Mireia Planas i Lisbona, Dmitry Berenson, et al. “Manipulation via Membranes: High-Resolution and Highly Deformable Tactile Sensing and Control”. In: *Conference on Robot Learning*. PMLR. 2023, pp. 1850–1859.
- [23] Stefan Escaida Navarro, Stephan Mühlbacher-Karrer, Hosam Alagi, et al. “Proximity perception in human-centered robotics: A survey on sensing systems and applications”. In: *IEEE Transactions on Robotics* 38.3 (2021), pp. 1599–1620.
- [24] Jessica Yin, Tess Hellebrekers, and Carmel Majidi. “Closing the Loop with Liquid-Metal Sensing Skin for Autonomous Soft Robot Gripping”. In: *2020 3rd IEEE International Conference on Soft Robotics (RoboSoft)*. 2020, pp. 661–667. DOI: 10.1109/RoboSoft48309.2020.9116000.
- [25] Tess Hellebrekers, Kadri Bugra Ozutemiz, Jessica Yin, et al. “Liquid Metal-Microelectronics Integration for a Sensorized Soft Robot Skin”. In: *2018 IEEE/RSJ International Conference on Intelligent Robots and Systems (IROS)*. IEEE. 2018, pp. 5924–5929.
- [26] Radhen Patel, Rebecca Cox, and Nikolaus Correll. “Integrated proximity, contact and force sensing using elastomer-embedded commodity proximity sensors”. In: *Autonomous Robots* 42 (2018), pp. 1443–1458.
- [27] Andrew SaLoutos, Elijah Stanger-Jones, Menglong Guo, et al. “Design of a Multimodal Fingertip Sensor for Dynamic Manipulation”. In: *arXiv preprint arXiv:2209.11368* (2022).
- [28] Andrew SaLoutos, Hongmin Kim, Elijah Stanger-Jones, et al. “Towards Robust Autonomous Grasping with Reflexes Using High-Bandwidth Sensing and Actuation”. In: *arXiv preprint arXiv:2209.11367* (2022).
- [29] Akihiko Yamaguchi and Christopher G Atkeson. “Combining finger vision and optical tactile sensing: Reducing and handling errors while cutting vegetables”. In: *2016 IEEE-RAS 16th International Conference on Humanoid Robots (Humanoids)*. IEEE. 2016, pp. 1045–1051.
- [30] Francois R Hogan, Michael Jenkin, Sahand Rezaei-Shoshtari, et al. “Seeing through your skin: Recognizing objects with a novel visuotactile sensor”. In: *Proceedings of the IEEE/CVF Winter Conference on Applications of Computer Vision*. 2021, pp. 1218–1227.
- [31] Francois R Hogan, Jean-François Tremblay, Bobak H Baghi, et al. “Finger-STS: Combined Proximity and Tactile Sensing for Robotic Manipulation”. In: *IEEE Robotics and Automation Letters* 7.4 (2022), pp. 10865–10872.
- [32] Quan Khanh Luu, Dinh Quang Nguyen, Nhan Huu Nguyen, et al. “Soft Robotic Link with Controllable Transparency for Vision-based Tactile and Proximity Sensing”. In: *arXiv preprint arXiv:2211.03253* (2022).
- [33] Jessica Yin, Gregory M Campbell, James Pikul, et al. “Multimodal proximity and visuotactile sensing with a selectively transmissive soft membrane”. In: *2022 IEEE 5th International Conference on Soft Robotics (RoboSoft)*. IEEE. 2022, pp. 802–808.

- [34] Yashraj S Narang, Karl Van Wyk, Arsalan Mousavian, et al. “Interpreting and predicting tactile signals via a physics-based and data-driven framework”. In: *arXiv preprint arXiv:2006.03777* (2020).
- [35] Carmelo Sferrazza, Adam Wahlsten, Camill Trueeb, et al. “Ground truth force distribution for learning-based tactile sensing: A finite element approach”. In: *IEEE Access* 7 (2019), pp. 173438–173449.
- [36] Raymond W Ogden, Giuseppe Saccomandi, and Ivonne Sgura. “Fitting hyperelastic models to experimental data”. In: *Computational Mechanics* 34.6 (2004), pp. 484–502.
- [37] R. Hopf, L. Bernardi, J. Menze, et al. “Experimental and theoretical analyses of the age-dependent large-strain behavior of Sylgard 184 (10:1) silicone elastomer”. In: *Journal of the Mechanical Behavior of Biomedical Materials* 60 (2016), pp. 425–437. ISSN: 1751-6161. DOI: <https://doi.org/10.1016/j.jmbbm.2016.02.022>. URL: <https://www.sciencedirect.com/science/article/pii/S1751616116000758>.
- [38] Daolin Ma, Elliott Donlon, Siyuan Dong, et al. “Dense tactile force estimation using GelSlim and inverse FEM”. In: *2019 International Conference on Robotics and Automation (ICRA)*. IEEE. 2019, pp. 5418–5424.
- [39] Naveen Kuppaswamy, Alejandro Castro, Calder Phillips-Grafflin, et al. “Fast model-based contact patch and pose estimation for highly deformable dense-geometry tactile sensors”. In: *IEEE Robotics and Automation Letters* 5.2 (2019), pp. 1811–1818.
- [40] Huichan Zhao, Kevin O’Brien, Shuo Li, et al. “Optoelectronically innervated soft prosthetic hand via stretchable optical waveguides”. In: *Science robotics* 1.1 (2016), eaai7529.
- [41] Yipai Du, Guanlan Zhang, Yazhan Zhang, et al. “High-resolution 3-dimensional contact deformation tracking for FingerVision sensor with dense random color pattern”. In: *IEEE Robotics and Automation Letters* 6.2 (2021), pp. 2147–2154.
- [42] Zilin Si and Wenzhen Yuan. “Taxim: An example-based simulation model for gelsight tactile sensors”. In: *IEEE Robotics and Automation Letters* 7.2 (2022), pp. 2361–2368.
- [43] Samarth Brahmabhatt, Cusuh Ham, Charles C Kemp, et al. “Contactdb: Analyzing and predicting grasp contact via thermal imaging”. In: *Proceedings of the IEEE/CVF conference on computer vision and pattern recognition*. 2019, pp. 8709–8719.
- [44] Arjun Lakshminpathy, Dominik Bauer, and Nancy S Pollard. “Contact tracing: A low cost reconstruction framework for surface contact interpolation”. In: *2021 IEEE/RSJ International Conference on Intelligent Robots and Systems (IROS)*. IEEE. 2021, pp. 5165–5172.
- [45] JH Pikul, S Li, H Bai, et al. “Stretchable surfaces with programmable 3D texture morphing for synthetic camouflaging skins”. In: *Science* 358.6360 (2017), pp. 210–214.
- [46] Robert Baines, Sree Kalyan Patiballa, Benjamin Gorissen, et al. “Programming 3D curves with discretely constrained cylindrical inflatables”. In: *Advanced Materials* (), p. 2300535.
- [47] Gregory M Campbell, Jessica Yin, Yuyang Song, et al. “Electroadhesive Clutches for Programmable Shape Morphing of Soft Actuators”. In: *2022 IEEE/RSJ International Conference on Intelligent Robots and Systems (IROS)*. IEEE. 2022, pp. 11594–11599.
- [48] Robert Baines, Sree Kalyan Patiballa, Joran Booth, et al. “Multi-environment robotic transitions through adaptive morphogenesis”. In: *Nature* 610.7931 (2022), pp. 283–289.
- [49] Aimee Goncalves, Naveen Kuppaswamy, Andrew Beaulieu, et al. “Punyo-1: Soft tactile-sensing upper-body robot for large object manipulation and physical human interaction”. In: *2022 IEEE 5th International Conference on Soft Robotics (RoboSoft)*. IEEE. 2022, pp. 844–851.
- [50] Qian-Yi Zhou, Jaesik Park, and Vladlen Koltun. “Open3D: A Modern Library for 3D Data Processing”. In: *arXiv:1801.09847* (2018).
- [51] Sudharshan Suresh, Maria Bauza, Kuan-Ting Yu, et al. “Tactile SLAM: Real-time inference of shape and pose from planar pushing”. In: *2021 IEEE International Conference on Robotics and Automation (ICRA)*. IEEE. 2021, pp. 11322–11328.
- [52] Jialiang Zhao, Maria Bauza, and Edward H Adelson. “FingerSLAM: Closed-loop Unknown Object Localization and Reconstruction from Visuo-tactile Feedback”. In: *arXiv preprint arXiv:2303.07997* (2023).